

# The Casimir effect in microstructured geometries

Alejandro W. Rodriguez<sup>1,2</sup>, Federico Capasso<sup>1\*</sup> and Steven G. Johnson<sup>2</sup>

**In 1948, Hendrik Casimir predicted that a generalized version of van der Waals forces would arise between two metal plates due to quantum fluctuations of the electromagnetic field. These forces become significant in micromechanical systems at submicrometre scales, such as in the adhesion between movable parts. The Casimir force, through a close connection to classical photonics, can depend strongly on the shapes and compositions of the objects, stimulating a decades-long search for geometries in which the force behaves very differently from the monotonic attractive force first predicted by Casimir. Recent theoretical and experimental developments have led to a new understanding of the force in complex microstructured geometries, including through recent theoretical predictions of Casimir repulsion between vacuum-separated metals, the stable suspension of objects and unusual non-additive and temperature effects, as well as experimental observations of repulsion in fluids, non-additive forces in nanotrench surfaces and the influence of new material choices.**

Fluctuation-induced electromagnetic forces between neutral bodies become more and more important as micromechanical and microfluidic devices enter submicrometre scales. These forces are known by several different names, depending on the regime in which they operate, including van der Waals, Casimir–Polder and, more generally, Casimir forces (of which van der Waals forces are special cases)<sup>1–4</sup>. Casimir forces arise from electromagnetic waves created by quantum and thermal fluctuations<sup>5–21</sup>. The dramatic progress made in the theoretical understanding and measurement of Casimir forces over the past ten years may soon allow them to be exploited in novel microelectromechanical systems (MEMS) and microfluidic devices<sup>8,22–24</sup>.

Experimentally, Casimir forces have been measured with ever greater precision<sup>25–34</sup> in microstructured geometries that increasingly deviate from the original parallel-plate configuration<sup>26</sup>. They have even been measured in fluids that allow the sign of the force to change<sup>35</sup>. Theoretically, the calculation of Casimir forces was traditionally limited to planar or near-planar geometries, but recent developments have led to a host of new computational methods capable of modelling arbitrary non-planar geometries with high accuracy<sup>36–45</sup>. This combined experimental and theoretical progress has allowed researchers to design geometries and materials that exhibit force phenomena significantly different from the well-known attraction between parallel plates. Such advances may lead to new regimes of operation for micromechanical devices<sup>8,46</sup> and may also provide new ways to combat unwanted interactions such as ‘stiction’ between moving parts. In this Review, we summarize the basic physics of Casimir and van der Waals interactions, discuss recent experimental systems, outline theoretical progress and consider some of the latest predictions of this unusual force phenomena.

## From van der Waals to Casimir forces

Van der Waals forces are a familiar concept from introductory physics and chemistry: two neutral particles have fluctuating dipole moments resulting from quantum or thermal effects, which, for a particle separation of  $d$ , lead to a  $d^{-6}$  interaction energy that is commonly used, for example, as a long-range attraction term when describing the interactions between atoms and molecules<sup>1–4</sup>. Physically, this attraction arises as shown in Fig. 1a; whenever one particle acquires a spontaneous dipole moment  $\mathbf{p}_1$ , the resulting dipole electric field (black lines) polarizes the adjacent particle to

produce an induced dipole moment  $\mathbf{p}_2 \sim d^{-3}$  (ref. 4). Assuming positive polarizabilities, the direction of the dipole fields means that these two dipoles are oriented so as to attract each other, with an interaction energy that scales as  $d^{-6}$ . This leads to the van der Waals ‘dispersion’ force, and similar considerations apply to particles with permanent dipole moments that can rotate freely. The key to more general considerations of Casimir physics is to understand that this  $d^{-6}$  picture of van der Waals forces makes two crucial approximations that are not always valid: it employs the quasi-static approximation to ignore wave effects, and also ignores multiple scattering if there are more than two particles.

The quasi-static approximation assumes that the dipole moment  $\mathbf{p}_1$  polarizes the second particle instantaneously, which is valid if  $d$  is much smaller than the typical wavelength of the fluctuating fields. However, the finite wave propagation speed of light must be taken into account when  $d$  is much larger than the typical wavelength, as shown in Fig. 1b, and it turns out that the resulting Casimir–Polder interaction energy asymptotically scales as  $d^{-7}$  for large  $d$  (ref. 47). More generally, the interaction is not a simple power law between these limits, but instead depends on an integral of fluctuations at all frequencies scaled by a frequency-dependent polarizability of the particles<sup>4</sup>.

The presence of multiple particles further complicates the situation because multiple scattering must be considered (Fig. 1b). For example, with three particles, the initial dipole  $\mathbf{p}_1$  will induce polarizations  $\mathbf{p}_2$  and  $\mathbf{p}_3$  in the other two particles, but  $\mathbf{p}_2$  will create its own field that further modifies  $\mathbf{p}_3$ , and so on. Thus, the interaction between multiple particles is generally non-additive, and there is no two-body force law that can simply be summed to incorporate all interactions. Multiple scattering is negligible for a sufficiently dilute gas or for weak polarizabilities<sup>4,48</sup>, but it becomes very significant for interactions between two (or more) solid bodies, which consist of many fluctuating dipole moments that all interact in a complicated way through electromagnetic radiation (Fig. 1c). When these multiple scattering effects are combined with wave retardation in a complete picture, they yield the Casimir force<sup>9</sup>.

Hendrik Casimir based his prediction on a simplified model involving two parallel perfectly conducting plates separated by a vacuum. Although the Casimir force arises from electromagnetic fluctuations, real photons are not involved. Quantum mechanically, these fluctuations can be described in terms of virtual photons of energy equal to the zero-point energies of the electromagnetic

<sup>1</sup>School of Engineering and Applied Sciences, Harvard University, Cambridge, Massachusetts 02138, USA. <sup>2</sup>Department of Mathematics, Massachusetts Institute of Technology, Cambridge, Massachusetts 02139, USA. \*e-mail: capasso@seas.harvard.edu

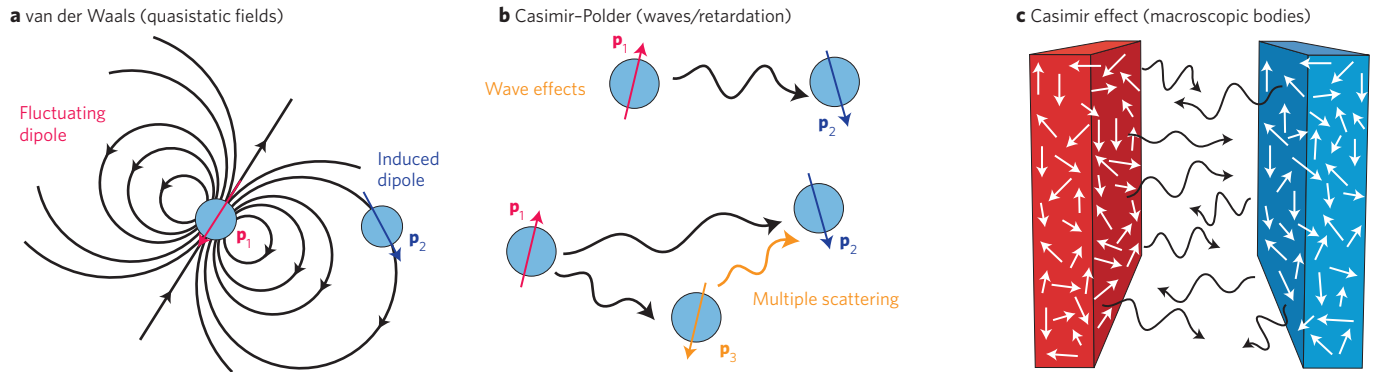


**Figure 1 | Relationship between van der Waals, Casimir-Polder and Casimir forces, whose origins lie in the quantum fluctuations of dipoles.**

**a.** A fluctuating dipole  $\mathbf{p}_1$  induces a fluctuating electromagnetic dipole field, which in turn induces a fluctuating dipole  $\mathbf{p}_2$  on a nearby particle, leading to van der Waals forces between the particles. **b.** When the particle spacing is large, retardation/wave effects modify the interaction, leading to Casimir-Polder forces. When more than two particles interact, the non-additive field interactions lead to a breakdown of the pairwise force laws. **c.** In situations consisting of macroscopic bodies, the interaction between the many fluctuating dipoles present within the bodies leads to Casimir forces.

modes of the system. By considering the contribution of the electromagnetic field modes to the zero-point energy ( $U$ ) of the parallel plate configuration, Casimir predicted an attractive force between the plates. Because only electromagnetic modes that have nodes on both walls can exist within the cavity, the mode frequencies ( $\omega$ ) depend on the separation between the plates, giving rise to a pressure of  $P_C = -\partial U/\partial d$  (ref. 9):

$$P_C = -\frac{\hbar c \pi^2}{240 d^4} = -\frac{1.3 \times 10^{-27} \text{ Nm}^2}{d^4} \quad (1)$$

where  $c$  is the vacuum speed of light and  $\hbar$  is the reduced Planck's constant. The force in this case is attractive because the mode density in free space is larger than that between the plates. Following Casimir's calculation, Lifshitz, Dzyaloshinskiĭ and Pitavskii considered the more general case of realistic dielectric plates by exploiting the fluctuation-dissipation theorem, which relates the dissipative properties of the plates (that is, the optical absorption resulting from the many microscopic dipoles in the plates) and the resulting electromagnetic fluctuations at equilibrium<sup>10</sup>. For realistic metallic plates separated by  $d$ , the force again scales as  $d^{-4}$  for large  $d$ . At small  $d$ , the force scales as  $d^{-3}$  (this is the quasi-static limit, where the coefficient is known as the Hamaker constant<sup>4</sup>), with a complicated intermediate  $d$ -dependence that is determined by the frequency-dependent permittivity ( $\epsilon$ ) of the materials. Here, 'small' and 'large'  $d$  are relative to a characteristic wavelength  $\lambda_0$ , which for metals is the plasma wavelength and is typically in the ultraviolet range (a few hundred nanometres). The geometry of the system can be used to greatly modify wave propagation beyond the simple planar regime, but a broad-bandwidth scattering calculation is required to capture the complete physics of such interactions<sup>38</sup>.

Although a complete description of the Casimir interaction between macroscopic bodies is beyond the level of this Review, it is instructive to consider the interaction energy between a single particle with polarizability  $\alpha$  and a macroscopic body<sup>7,47</sup>. The particle can be thought of as a fluctuating dipole moment  $\mathbf{p}$  (proportional to  $\text{Im}(\alpha)$ , the dissipation), which generates electromagnetic fields that propagate outwards, scatter off the body and then return to the location of the particle, producing a total field  $\mathbf{E}$  (the 'Green's function') and an energy  $-\mathbf{p} \cdot \mathbf{E}$ . To compute the interaction of the dipole with the body, one subtracts the field  $\mathbf{E}_0$  produced by an isolated dipole to obtain an interaction energy

$U \sim -\mathbf{p} \cdot (\mathbf{E} - \mathbf{E}_0)$ , which is finite even for a point dipole (whereas  $\mathbf{E}$  and  $\mathbf{E}_0$  themselves diverge at the source point). This energy must be integrated over fluctuations at all frequencies, multiplied by an appropriate frequency distribution such as a Bose-Einstein distribution, which includes the effects of thermal fluctuations at non-zero temperatures. The key fact is that computing Casimir interactions reduces to solving classical scattering problems, and this fact carries over to more general problems involving interactions between macroscopic bodies — such bodies consist of many such dipoles, and correspondingly one must solve many scattering problems for many current sources or incident waves. This has three consequences, which are discussed in more detail below. First, it is evident that standard computational techniques from classical electromagnetism can be used to solve for the Green's function and hence the Casimir energy, although many classical problems must be solved to yield a single  $U$ . Second, the non-additivity is clear because classical scattering involves solving the full Maxwell's equations, and simply summing the individually scattered fields from each body is rarely accurate. Finally, the scattered field  $\mathbf{E}$  is a rapidly oscillating function of  $\omega$  because of interference effects, thus requiring a highly oscillatory integral over a broad bandwidth to obtain the total force; this has dramatic implications for the conceptual and computational frameworks that must be used to understand and calculate Casimir phenomena, as explained in Box 1.

### Experimental validations

The pioneering experiments of Spaarnay<sup>49</sup> were not able to unambiguously confirm the existence of the Casimir force because of (among other factors) the large error arising from the difficulty in maintaining a high degree of parallelism between the plates (later solved using a sphere-plate geometry; Fig. 2). Three important points must be taken into account when making precise Casimir force measurements<sup>50</sup>. First, in practice there is always an electrostatic potential difference between the two surfaces ( $V_0$ ) that arises from the presence of different metals in the electrical circuit connecting the two surfaces, different work functions between the thin films and other electrostatic effects<sup>34,50,51</sup>. Residual electrostatic forces must be cancelled by applying a voltage of the same magnitude but opposite polarity, usually ranging from a few mV to  $\sim 100$  mV. Second, although the relative distance  $d$  between the surfaces is controlled by a piezoelectric transducer, the initial separation between the two interacting surfaces  $d_0$  is *a priori* unknown (Fig. 2c), and therefore the absolute separation ( $d - d_0$ ) must be

obtained from a calibration procedure<sup>8,50</sup>. Finally, the electronic signal coming out of the measurement set-up must be converted to a force. It is therefore necessary to calibrate the instrument with a controlled force, usually an electrostatic one.

Accurate comparison between theory and experiments is subject to other challenges, particularly at distances below a few hundred nanometres. Because the Casimir force depends on the optical properties  $\epsilon$  of the materials — in particular  $\epsilon$  at imaginary frequencies — an accurate knowledge of  $\text{Im}(\epsilon)$  is necessary over a wide spectral range. Even though these data are available for metals such as gold, they do not correspond to any single gold film but rather have been assembled from different authors who have performed measurements on different samples using different deposition processes to cover a large frequency range. A high-precision comparison between Casimir theory and measurements would require characterization of the thin films actually used in the force experiments, and uncertainties in the knowledge of  $\epsilon$  alone can lead to significant uncertainties in the force calculation<sup>52–54</sup>. Another important factor is a knowledge of the surface roughness, which tends to enhance the measured force with respect to a flat surface<sup>27,55–57</sup>. Accurate surface roughness profiles over a large

area can be obtained by interferometric methods<sup>8</sup> using an optical profilometer, yielding a statistical model of the roughness that can be used to correct the Casimir theory<sup>58</sup>. Finally, primarily at larger (micrometre) separations, there is a temperature correction to the Casimir force associated with the presence of thermal photons<sup>16,17,59</sup>, which is discussed further below.

For ideal metals and sphere–plate separations  $d$  much smaller than the sphere radius  $R$ , the zero-temperature Casimir force is

$$F_C = -\frac{\hbar c \pi^3 R}{360 d^3} \quad (2)$$

which is independent of the plate area<sup>60</sup>. Measurements for dielectric bodies in this geometry were first reported by Derjaguin and Abrikossova<sup>28</sup>. Metallic films are more difficult to use in experiments than dielectric surfaces (which can exploit optical techniques for alignment and distance measurements). The first clear experimental evidence of the Casimir effect between metallic surfaces was presented by van Blokland and Overbeek<sup>34</sup>, while the first high-precision (5% accuracy) measurements were reported by Lamoreaux

### Box 1 | Imaginary frequencies and the disappearance of resonances

Much of classical photonics design centres around narrow-bandwidth effects<sup>121</sup> such as resonant cavities for filters and enhanced light–matter interactions, interference effects such as Mach–Zehnder interferometers and diffraction gratings, and even resonances arising in exotic ‘metamaterials’ that lead to negative effective indices. Because the Casimir energy is a result of broad-bandwidth electromagnetic fluctuations, most standard photonics phenomena tend to cancel out. In particular, looking at the energy or force contributions within a narrow bandwidth of  $\omega$  can be very deceptive. Even if the force contributions seem to be dramatically altered within a narrow bandwidth, say by a resonant effect, this alteration is usually mostly cancelled by contributions at other frequencies. How then, can one think about (or even compute) the Casimir force? The answer comes from complex analysis: because the force contributions are related to causal scattering problems, they are analytic functions (no poles) in the upper-half complex frequency plane ( $\text{Im}(\omega) > 0$ ), and it is mathematically equivalent (by contour integration) to integrate contributions for all imaginary frequencies  $\omega = i\kappa$  instead of for all real frequencies (that is, in the Laplace domain rather than the Fourier domain). At imaginary frequencies, the force contributions are smooth, mostly non-oscillatory, and exponentially decaying. This is because a field  $r$  away from a dipole source oscillating at frequency  $\omega$  is a spherical wave  $\sim e^{i\omega r/c}/r$  for real  $\omega$ , but is exponentially decaying  $\sim e^{-\kappa r/c}/r$  for  $\omega = i\kappa$ , so at imaginary frequencies there are no oscillations, wave interference effects or resonances (Fig. B1). Although currents and fields become exponentially growing quantities in time for  $\omega = i\kappa$ , the exponential time dependence is not a computational obstacle if the fields are viewed and computed in the frequency domain. Correspondingly, the relevant material responses are the permittivities  $\epsilon(i\kappa)$  at imaginary frequencies, for which all resonant effects disappear; for example, a Lorentzian absorption line at real frequencies becomes a monotonically decaying real  $\epsilon$  at  $\omega = i\kappa$ . This is unfamiliar ground in classical photonics, but is crucial for Casimir physics — almost all theoretical work in this field relies on such an imaginary-frequency perspective. Thus, modifying the Casimir force requires the force integrand to be changed over a broad range of imaginary frequencies, in which case it is impossible to rely on wave-interference effects like resonances

or diffraction. For example, metamaterials, which rely strongly on resonances to create exotic ‘effective’ materials and were initially suggested to strongly alter Casimir interactions<sup>122–124</sup>, turn out to have minimal effect when the full spectrum and realistic microstructures are considered<sup>125,126</sup>.

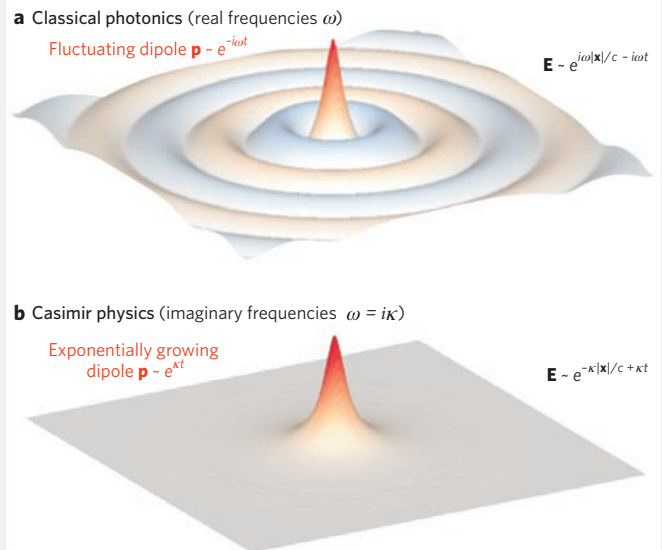


**Figure B1 | Illustration of the conceptual difference underlying the physics of narrow-bandwidth classical photonic phenomena, best viewed at real frequencies  $\omega$ , and broad-bandwidth quantum electromagnetic fluctuations (Casimir forces), best viewed at imaginary frequencies  $i\kappa$ .** **a**, Electric field induced by a dipole source oscillating at real frequency  $\omega$ , showing spatial oscillations that decay away from the dipole. **b**, The field induced by the same dipole source evaluated at imaginary frequency  $\omega = i\kappa$  (corresponding to an exponentially growing dipole in time) is now strictly exponentially decaying in space.

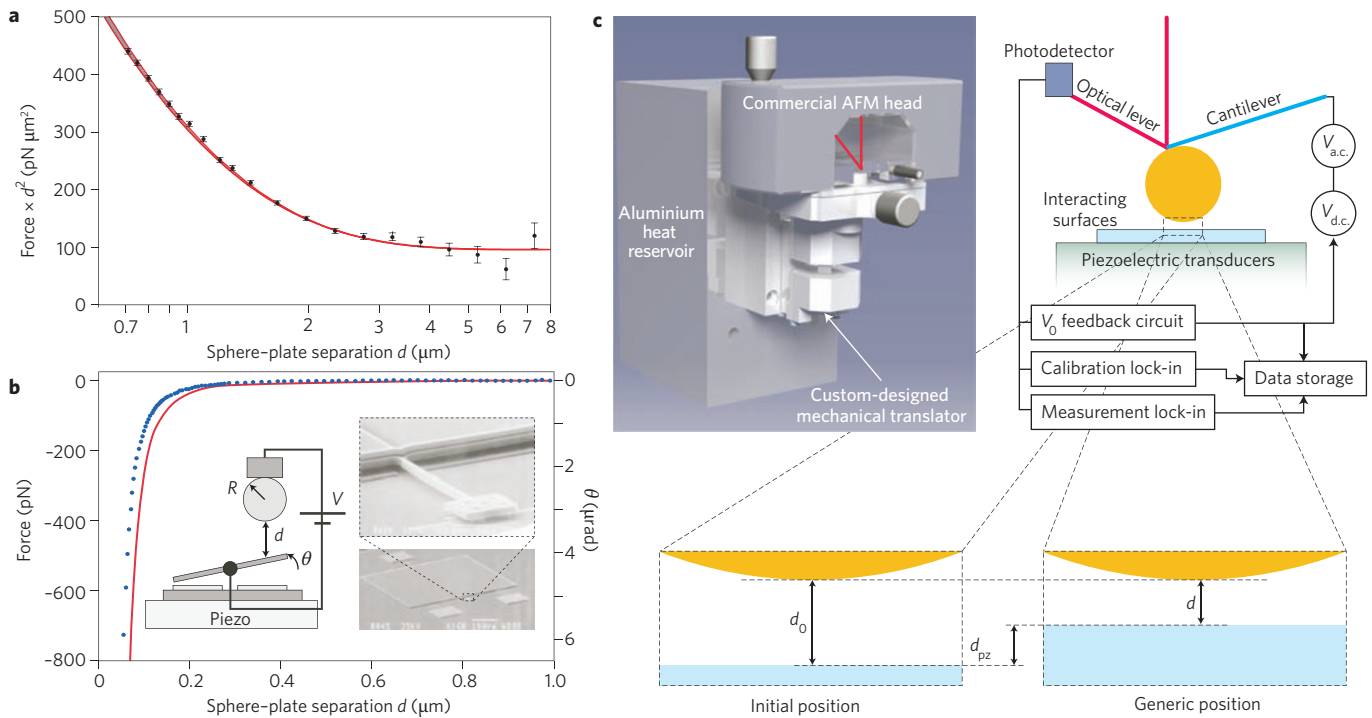


**Figure 2 | Results and set-ups of various experiments that have measured Casimir forces in the sphere-plate geometry.** **a**, Experimentally measured Casimir force between a gold-coated spherical surface (radius 15.6 cm) and a gold-coated slab, multiplied by the square of their surface-surface separation  $d$  and plotted in the 0.7–7  $\mu\text{m}$  range<sup>33</sup>. The force is compared with predictions from Lifshitz theory (red curve). The plateau in the data at distances of  $\geq 3 \mu\text{m}$  shows the dominant role of the thermal Casimir force at these distances. **b**, Experimentally measured Casimir force between a sphere and plate in the MEMS of ref. 65. The red curve shows the corresponding calculated force in the ideal case of perfect metals (no roughness or real-dielectric corrections). Inset: Casimir force detection set-up, including a scanning electron microscope micrograph of the torsional device used to measure the Casimir force. As the metallic sphere (mounted on the torsional device) approaches the plate, the Casimir force causes the plate to rotate. **c**, Set-up of the sphere-plate experiment of ref. 50, along with definitions of the initial separation ( $d_0$ ), piezoelectric-stage displacement ( $d_{pz}$ ) and surface-surface separation  $d$ . The displacement of the sphere is determined by measuring the light reflected from the cantilever. Figure reproduced with permission from: **a**, ref. 33, © 2011 NPG; **b**, ref. 65, © 2001 AAAS; **c**, ref. 50, © 2009 APS.

in 1997 using a torsional pendulum and surfaces coated with 0.5- $\mu\text{m}$ -thick gold<sup>31</sup>. Figure 2a shows Lamoreaux’s force data for a similar but more recent experiment<sup>33</sup> that corrects for calibration and other systematic errors in the original 1997 experiment, showing good agreement with the theoretical predictions in the 0.7–7  $\mu\text{m}$  separation range. From the data, one can observe that for separations of  $\leq 1 \mu\text{m}$ , the force due to zero-point energy fluctuations is much greater than the Casimir force associated with thermal fluctuations of the electromagnetic field, which scales as  $k_B TR/d^2$ , where  $k_B$  is the Boltzmann constant<sup>33</sup>. However, the thermal Casimir force dominates at separations greater than 3  $\mu\text{m}$ , as can be seen from the plateau in Fig. 2a.

In 2002, Bressi *et al.* unambiguously verified the Casimir force in the parallel-plate geometry<sup>25</sup> — over fifty years after Casimir’s original prediction. In their set-up, the two parallel surfaces comprised a chromium-coated cantilever beam that was free to oscillate around its clamping point, and a thicker beam (also chromium-coated) that was rigidly connected to a moveable frame, thereby allowing the distance from the cantilever to be adjusted. The displacement was measured interferometrically with a fibre facet on the opposite side of the cantilever, and electrostatic calibrations were performed by measuring the voltage between the source and the cantilever (which together form a capacitor), or alternatively by capacitance measurements using an a.c. bridge. The skin-depth of chromium ( $\sim 10 \text{ nm}$ ) is negligible and the ideal-metal Casimir force of equation (1) is approximately valid for the 0.5–3.0  $\mu\text{m}$  separations used. The measured pressure law was

$\sim (1.22 \pm 0.18) \times 10^{-27} \text{ N m}^2 \text{ d}^{-4}$ , which is in good agreement with equation (1).

Several additional approaches to high-precision Casimir measurements have been developed so far — primarily for sphere-plate geometries — using torsional balances, modified atomic force microscope (AFM) set-ups and MEMS.

Experimental techniques have now been sufficiently refined to detect patch potentials — small, random variations in the surface potential resulting from material strains, impurities and other irregularities, which lead to a  $d$ -dependent electrostatic potential  $V_0$  that limits the accuracy of Casimir force measurements. This  $d$ -dependent  $V_0$  was recently unambiguously observed in a number of experiments between metal-coated plate and sphere surfaces, and has also been systematically modelled<sup>51</sup>.

AFM-type measurements involve attaching a sphere or cylinder (diameter of tens of micrometres or more) to the cantilever, whose distance from another surface is changed using a piezoelectric controller<sup>32,50,61,62</sup>. The cantilever deflection, which is proportional to the force between the surfaces, is detected by measuring the deflection of a laser beam bouncing off the top of the cantilever. An advanced AFM experiment<sup>50</sup> is shown in Fig. 2c, involving a 100- $\mu\text{m}$ -radius gold-coated sphere and a metal-coated glass plate mounted on a capacitive feedback-controlled piezoelectric transducer. This experiment was able to detect a 40–50% decrease in the Casimir force at 50–150 nm separations when switching between a gold-coated plate and an indium tin oxide (ITO)-coated plate<sup>50</sup>, primarily thanks to the smaller plasma frequency of ITO.

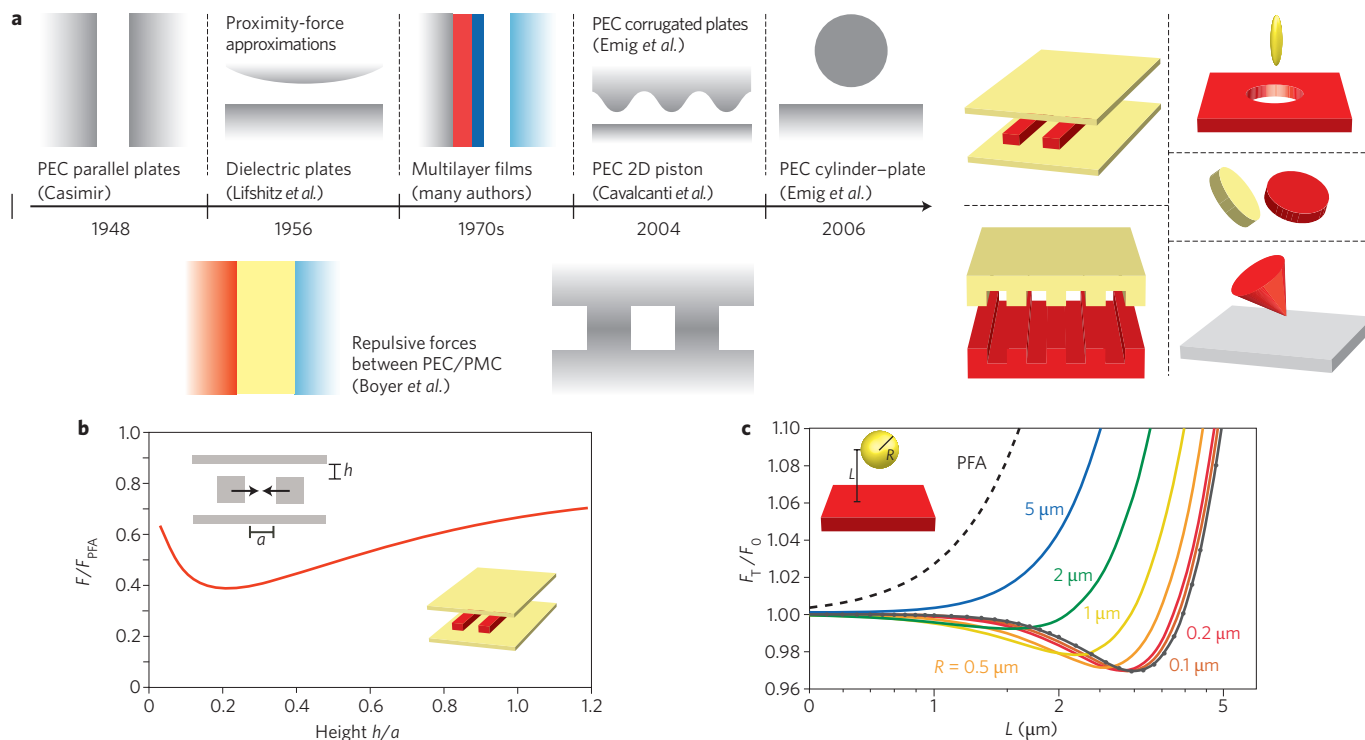


**Figure 3 | Theoretical developments in the study of the influence of geometry and material choice on the Casimir force.** **a**, Left: timeline of selected theoretical Casimir-force calculations since 1948, mostly restricted to planar or simple geometries involving perfectly electric conductors (PEC) and perfectly magnetic conductors (PMC). Right: collage of various complex geometries studied since 2007 using recently proposed and robust theoretical methods, including two waveguides adjacent to semi-infinite plates<sup>93</sup>, an ellipsoidal nanoparticle above a plate with a hole<sup>101</sup>, rotated hockey pucks<sup>90</sup>, trench gratings<sup>86,120</sup> and a cone at an angle from a plate<sup>94</sup>. These new theoretical tools have enabled the study of geometries in which the non-additivity of the Casimir force leads to qualitatively interesting effects. **b**, Casimir force per unit length  $F$  between two metallic waveguides (red blocks) separated by a distance  $a$ , divided by the force  $F_{PFA}$  predicted by the PFA, as a function of their height  $h$  from two adjacent metal plates (yellow).  $F_{PFA}$  predicts an  $h$ -independent force between the waveguides (the pressure between flat plates multiplied by the interior area of the waveguides); thus, the non-monotonic dependence is a signature of the multi-body (non-additive) nature of the Casimir force. **c**, Casimir force  $F_T$  between a metallic sphere and a plate at room temperature, divided by the force at zero temperature  $F_0$ , as a function of their separation  $L$ . Solid lines from the bottom to the top correspond to increasing values of sphere radius  $R$ ; the dotted curve corresponds to a sphere of radius  $R \ll L$ . The dashed curve represents the same force ratio, but as computed by the PFA, which fails to capture the non-monotonic dependence that appears as  $R$  decreases. Figure **c** reproduced with permission from ref. 97, © 2010 APS.

The ability to halve the Casimir force by coating a surface with widely available conductive oxides is expected to be important for many applications.

The authors of refs 63,64 recently showed that the Casimir force spatial gradient between a sphere and a plate can be measured without direct contact, which normally causes irreversible deterioration of the probe and the studied surface.

MEMS, typically silicon-integrated circuits with movable parts, have proven useful for Casimir force measurements<sup>8,65</sup>. The inset of Fig. 2b shows a prototypical device: a 500  $\mu\text{m}^2$  doped polysilicon plate suspended from two of its opposite sides by thin torsional rods. Two fixed polysilicon electrodes are located symmetrically underneath the plate — one on each side of the torsional rod. The top plate is therefore free to rotate about the torsional rods in response to an external torque. A schematic of the actuation mechanism based on the Casimir force is shown in Fig. 2b. The polystyrene sphere has a radius of 100  $\mu\text{m}$  and is covered by a 200-nm-thick gold film. This technique has provided force sensitivities of a few piconewtons — comparable to that of AFM-type set-ups<sup>32,50,61</sup>. Figure 2b shows the results of that measurement alongside the ideal-metal red curve of equation (2). The difference results from the finite permittivity and surface roughness (tens of nanometres); theoretical calculations incorporating these corrections are in very good agreement with experiments<sup>65</sup>.

Realistic calculations of the Casimir force must also include corrections for non-zero temperatures (the thermal Casimir force), and an interesting prediction is that the finite conductivity of a real metal, as described by the Drude model, has a significant impact on these corrections<sup>66</sup>. Various experiments, complicated by the many uncertainties discussed above, have attempted to observe this impact, and controversy has arisen because some experiments claim not to observe this correction<sup>58,67</sup>. However, a recent experiment by the Lamoreaux group<sup>33</sup> — the first to report high-precision measurements for separations of more than 3  $\mu\text{m}$ , where thermal effects are dominant — indicates an agreement with the Drude model. In the context of Casimir forces in complex microstructures, however, most efforts have focused on achieving qualitative changes in the force behaviour that are not dependent on the precise nature of these small (typically <5%) corrections.

### Recent theoretical progress

Researchers did not stray far from the parallel-plate geometry in the first 50 years after Casimir's prediction<sup>9</sup>. Lifshitz, Pitaevskii, Dzyaloshinskiĭ and others generalized Casimir's work to arbitrary dielectric materials<sup>10,11</sup> and eventually to arbitrary multilayer-film geometries (where the Casimir force can be related to the classical reflection spectrum)<sup>68–70</sup>. Although exotic materials such as perfect

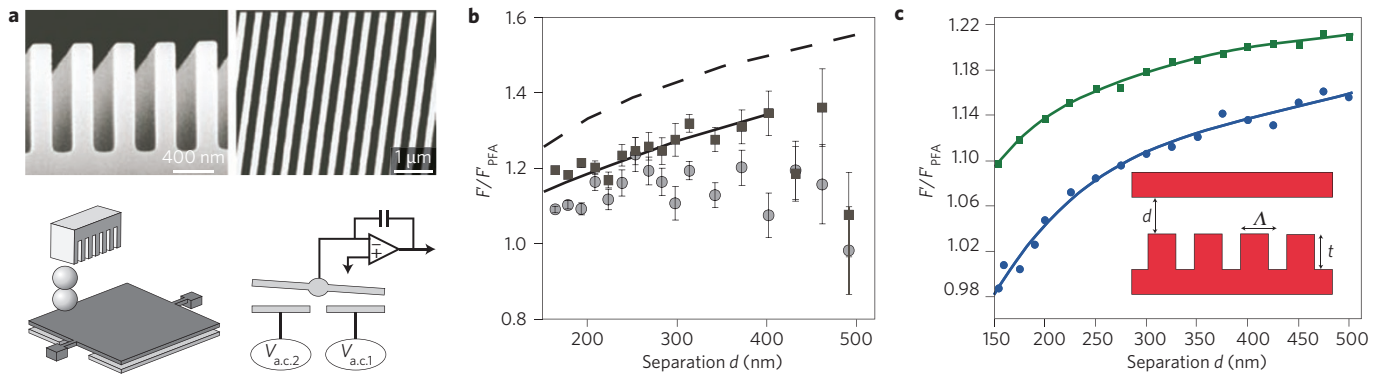


**Figure 4 | Experimental and theoretical works on a nanotrench geometry in which the Casimir force deviates significantly from the predictions of the PFA.** **a**, Lateral (upper-left panel) and top (upper-right panel) cross-sections of the rectangular trench geometry studied in ref. 26: a silicon trench of periodicity  $\Lambda = 400$  nm and depth  $t = 0.98$   $\mu\text{m}$  is suspended by a distance  $d$  above two stacked  $50$   $\mu\text{m}$  glass spheres mounted on a movable  $3.5$ - $\mu\text{m}$ -thick,  $500$   $\mu\text{m}^2$  silicon plate. A schematic of the experimental set-up is also shown (lower panels). **b**, Ratio  $F/F_{\text{PFA}}$  of the measured Casimir force gradient between the sphere and the grating to the force gradient expected from the PFA, for samples A ( $2\Lambda/t = 1.87$ , circles) and B ( $2\Lambda/t = 0.82$ , squares), respectively. The Casimir force gradient was measured from the shifts in the resonant frequency of the oscillator (movable plate) and the results show strong (up to 20%) deviations from the PFA predictions. Theoretical values obtained in the ideal case of perfectly conducting surfaces<sup>110</sup> are plotted as the solid ( $2\Lambda/t = 2$ ) and dashed ( $2\Lambda/t = 1$ ) lines. The experiment shows conclusive evidence of the strong geometry dependence and non-additivity of the Casimir force. **c**,  $F/F_{\text{PFA}}$  for samples A (blue circles) and B (green squares) computed using a recently developed scattering method that incorporates material (experimental  $\epsilon$ ) effects<sup>86</sup>. Figure reproduced with permission from: **a,b**, ref. 26, © 2008 APS; **c**, ref. 86, © 2008 APS.

magnetic conductors<sup>71</sup> were considered, the geometries remained mostly planar. Forces in nearly planar geometries, such as a sphere and a plate with separation much smaller than the radius<sup>68,72,73</sup> (as in equation (2)), were also considered in a lowest-order approximation known as the proximity force approximation (PFA)<sup>60</sup>, in which the force per unit area of an equivalent parallel-plate geometry is summed for all adjacent surfaces (also called a pairwise additive approximation). For dilute or weakly polarizable media, alternative methods employed the Casimir–Polder approximation, which involves summing pairwise particle–particle interactions<sup>74,75</sup>. Only a few artificial non-planar geometries admit semi-analytical solutions, such as the hollow perfect-metal spherical shell<sup>6,76,77</sup> or the ‘Casimir piston’, which consists of two perfect-metal blocks sliding between perfect-metal walls<sup>78–80</sup>. Self-energies were computed semi-analytically for the perfect-metal box<sup>6</sup> and sphere configurations<sup>76,77</sup> and seemed to predict a repulsive (expansion-inducing) self-force, but these predictions turned out to be problematic: the repulsion disappears if the object is cut in half<sup>81</sup> or is cutoff-dependent<sup>82</sup>, or if the box expansion is replaced by the rigid ‘piston’ motion of one wall<sup>79</sup>. A crude timeline of these developments is shown in Fig. 3a.

Over the past ten years, a number of techniques have been demonstrated that can accurately predict Casimir interactions for arbitrary geometries and materials, limited only by the available computational power<sup>38</sup>. These techniques began with pioneering results for corrugated surfaces<sup>83</sup> and cylinder–plate geometries<sup>84,85</sup>, and have recently led to solutions for a plethora of complex three-dimensional structures (Fig. 3a, right). Like the single-particle example outlined above, these new techniques ultimately reduce to solving many classical scattering problems, such as computing the fields in response to a complete set of current sources<sup>40,41,44,45</sup> or incident waves (for example, a set of spherical or plane waves)<sup>36,39,42,48,85–89</sup>. Although the most intuitive connection to scattering problems arises from the physical fluctuating dipoles in the materials, most recent techniques have more subtle (but ultimately equivalent) derivations ranging from path integrals<sup>36,42,90</sup> to the statistics of photon fluctuations<sup>44</sup>, all of which reduce the problem to a smaller number of scattering problems involving sources or incident waves only on surfaces around the bodies, instead of within entire volumes. These approaches can be crudely divided into two

main categories: those that are mainly oriented towards semi-analytical study by exploiting symmetries of specific geometries and expanding incoming/outgoing waves in a Fourier-like basis (analogous to classical Mie scattering), and those that use localized current sources and generic grids/meshes (analogous to finite-difference/finite-element and boundary-element methods in classical electromagnetism)<sup>40,41,43,45,91</sup>. Ref. 38 provides a thorough review that emphasizes the connections to classical techniques, including two key differences from classical computations: that the results are integrated in some fashion over imaginary frequencies, and that multiple scattering solutions must also be combined in unfamiliar ways to obtain a single force.

### Recent theoretical predictions

Although Casimir calculations tend to be more computationally intensive than classical photonics simulations owing to the large number of classical scattering problems that must be solved to compute a single force, recent work has demonstrated that a wide variety of highly non-planar geometries can be modelled exactly, starting from early solutions for corrugated plate<sup>83</sup>, cylinder–plate<sup>84</sup>, eccentric cylinders<sup>88</sup>, sphere–plate<sup>92</sup> and sphere–sphere<sup>36</sup> geometries, extending to piston-like suspended-waveguide geometries<sup>93</sup>, corrugated dielectrics<sup>22,86</sup> and even cones<sup>94</sup> and fluid-suspended objects<sup>90,95</sup> with realistic permeable materials. The goal of much of this recent theoretical work has been to identify new geometries in which Casimir interactions behave in ways that differ qualitatively from the 1948 monotonic power-law attraction between parallel plates and that differ substantially from the PFA picture of pairwise surface–surface attractions. A small sampling of recent work that exploits the generality of these new numerical developments, including non-additive or unusual Casimir phenomena, is shown in Fig. 3. By breaking translation symmetry with corrugated surfaces, one can induce lateral forces<sup>83,86</sup>. For two waveguides sandwiched between parallel plates or suspended above a single plate, there is a non-additive effect in which the presence of the plate(s) non-monotonically alters the attraction between the waveguides as a function of plate–waveguide separation<sup>93,96</sup>. More recently, the ratio of the sphere–plate force at temperatures of 0 K and 300 K was found to depend non-monotonically on the

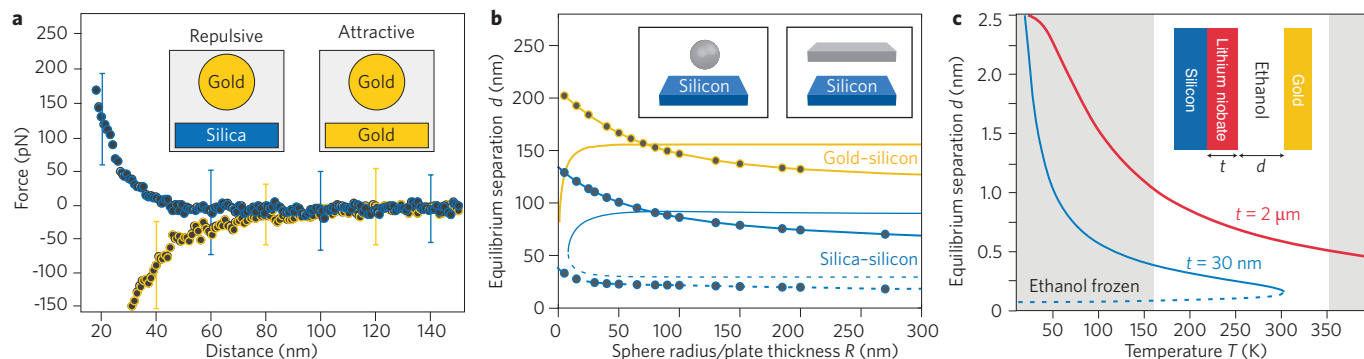


**Figure 5 | Experimental and theoretical works demonstrating the possibility of achieving Casimir repulsion, stable suspension of objects and large temperature effects in fluids.** **a**, Measured repulsive (blue) or attractive (yellow) Casimir force between a gold-coated (100 nm) polystyrene sphere and a silica (blue) or gold-coated (yellow) plate immersed in bromobenzene<sup>35</sup>. Circles represent the average force, averaged over 50 data sets, with corresponding error bars. **b**, Stable (solid) and unstable (dashed) equilibrium surface-surface separation  $d$  between a semi-infinite silicon slab and a sphere (circles) or film (lines) of radius or thickness  $R$ , immersed in ethanol, as a function of  $R$ . Yellow and blue lines denote gold and silica spheres/films, respectively. The dramatic sensitivity of  $d$  to the choice of material and geometry is a consequence of the strong interplay between material and geometric dispersion: depending on the choice of material, decreasing the thickness of a film can lead to the decrease and eventual disappearance of its stable  $d$  with the silicon plate, whereas decreasing the radius of a sphere, regardless of the material, acts to increase  $d$ . **c**, Stable (solid) and unstable (dashed)  $d$  between a semi-infinite gold slab and a layered lithium niobate (LiNbO<sub>3</sub>)-on-silicon substrate immersed in ethanol, as a function of temperature  $T$ . Red and blue lines correspond to the different LiNbO<sub>3</sub> thicknesses of  $t = 30$  nm and  $t = 2$   $\mu$ m, respectively. As shown,  $d$  is very sensitive to  $T$ , and can change dramatically and even disappear as  $T$  is changed. Figure reproduced with permission from: **a**, ref. 35, © 2009 NPG; **b**, ref. 95, © 2010 APS, **c**, ref. 114, © 2010 APS.

sphere-plate separation — a non-trivial interplay between geometry and temperature that is absent in pairwise approximations<sup>97,98</sup>. Both of these non-monotonic effects are depicted in Fig. 3.

Over the past five years, much progress has been made in answering the longstanding question of whether and how the Casimir force between two objects can become repulsive from the system geometry alone. For example, one theorem now states that mirror-symmetric geometries involving vacuum-separated objects can never lead to repulsive forces<sup>99</sup>, nor can vacuum-separated metal/dielectric objects ever be suspended in a stable non-touching equilibrium because of Casimir forces alone<sup>100</sup>. However, it is still possible to change the sign of the force merely by changing the geometry; repulsion was recently demonstrated between a needle-like metallic particle and a metal plate with a hole<sup>101</sup>. Repulsion can also arise in circumstances involving interleaved objects because of the trivial competition between pairwise attractive interactions (lateral forces) between surfaces<sup>22</sup>.

In addition to forces, quantum fluctuations can also induce torques on objects that are free to rotate<sup>8</sup>. This possibility was first studied theoretically in geometries consisting of planar objects with anisotropic materials<sup>102–104</sup>, and recently in more complicated geometries involving corrugated metallic surfaces<sup>105</sup>, dilute rectangular objects suspended above plates<sup>106</sup>, and eccentric metallic waveguides<sup>107</sup>.

### Emerging experimental regimes

The combination of new theoretical tools and experimental capabilities at submicrometre scales has led to a growing number of experiments that probe the geometry and material dependence of Casimir interactions outside of the planar metallic regime.

**Controlling film thickness.** One of the simplest ways of tailoring the Casimir force is to use films of varying thickness<sup>8,62,108,109</sup>. At submicrometre distances, the Casimir force depends on the reflectivity of the interacting surfaces for wavelengths in the ultraviolet to the far-infrared. The attraction between transparent materials is expected to be smaller than that between highly reflective mirrors because of the lower effective confinement of electromagnetic

modes inside the optical cavity (as is the case for ITO compared with gold)<sup>50</sup>. A thin metallic film can be transparent to electromagnetic waves that would otherwise be reflected by the bulk metal, particularly when the film thickness is much smaller than the material skin depth<sup>62,108,109</sup>. Consequently, the Casimir force on a metallic film is significantly reduced when its thickness is smaller than the skin depth of the bulk metal at ultraviolet to infrared wavelengths. For most common metals, this condition is reached when the layer thickness is around 10 nm.

Demonstrating the skin-depth effect requires the thickness and surface roughness of the film to be carefully controlled. The experiment described in ref. 8 involved coating a sphere with a 9.23-nm-thick film of palladium. The sphere was imaged with an optical profiler to determine its roughness. After Casimir force measurements between the sphere and a metal-coated flat surface had been made, the sphere was removed from the experimental apparatus, coated with an additional 200 nm of palladium and analysed with the optical profiler. Repeated measurements showed that the Casimir force was larger with the thicker palladium film, by an amount that was in good agreement with the Lifshitz theory<sup>8</sup>.

**Surface nanostructuring.** A recent experiment by Chan and co-workers<sup>26</sup> reported measurements of the Casimir force between nanostructured silicon surfaces (periodic rectangular trenches) and a gold-coated sphere (Fig. 4a), clearly showing the non-additivity of the Casimir force. Consider the interaction between a trench array, of trench periodicity  $\Lambda$  and depth  $t$ , and a parallel flat surface placed a distance  $d$  away from the top surface of the trenches. Under the PFA, the total pressure is  $P = pP_C$ , where  $p$  is the fraction of solid trench area exposed to the plate and  $P_C$  is the Casimir pressure between two flat infinite surfaces. Such an additive approximation is only expected to be accurate when the deviation from a parallel-plate geometry (the source of PFA) is controlled by a small parameter, for example in the limits of  $t \ll d$  or  $d \ll \Lambda$ . Computing the exact force in this geometry recently became possible using the modern methods outlined above, and was performed first for perfect metals<sup>110</sup> and later for realistic  $\epsilon$  values (ref. 86). As expected, strong deviations ( $\sim 20\%$ ) from PFA were observed for  $d$  comparable to  $\Lambda$  (Fig. 4b); however, exact

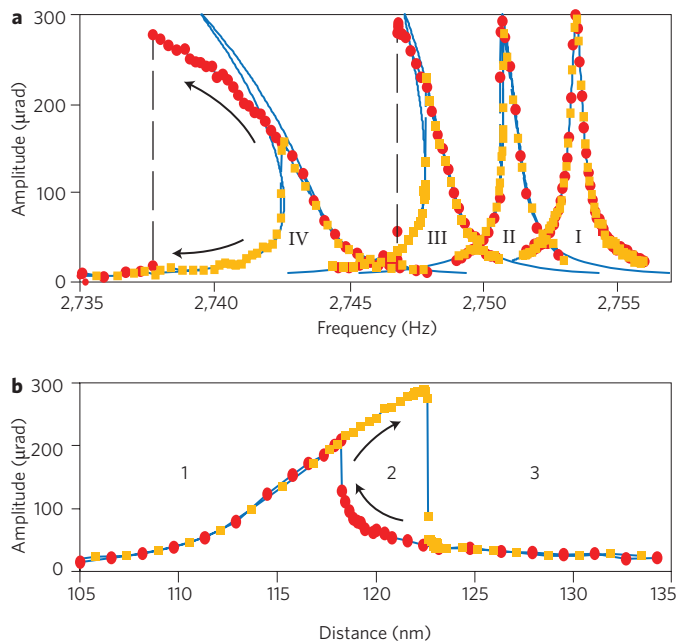


**Figure 6 | Experimental demonstration of the influence of the Casimir effect on the micromechanical torsional-oscillator device of ref. 46 (shown in Fig. 2b).** **a**, A torsional mode oscillation is excited by applying a driving voltage to an electrode under one plate. The measured amplitude versus frequency response for sphere-plate distances  $d$  of a few micrometres shows a resonance peak that is characteristic of a driven harmonic oscillator (peak I), regardless of whether the frequency is swept up (orange squares) or down (red circles). The resonance peak shifts to lower frequencies (peaks II, III and IV) by an amount that is consistent with the distance dependence of the Casimir force when the sphere is brought closer to the plate. **b**, The oscillator is excited at a fixed frequency and the amplitude response is measured as a function of  $d$ . As  $d$  changes, the resonance peak shifts because of the changing force gradient. In region 1, the fixed excitation frequency is higher than resonance frequency, and vice versa for region 3. In region 2, the amplitude of oscillation depends on the history of the plate position, a hysteresis effect induced by the Casimir force; depending on whether the plate was in region 1 or region 3 before it enters region 2, the amplitude of oscillation differs by up to a factor of 6. Figure reproduced with permission from ref. 46, © 2001 APS.

calculations demonstrate reasonable agreement (Fig. 4c). To attain such sensitivity, researchers measured the Casimir force gradient through shifts in the oscillation frequency of a torsional oscillator, on which the sphere was mounted. More recently, measurements of the lateral Casimir force between two corrugated metal plates produced an even larger deviation from PFA<sup>111</sup>, although the definition of PFA is particularly ambiguous for such lateral forces.

**Repulsion and suspension effects in fluids.** In fluid-separated situations, it has been known for decades that even planar geometries can exhibit repulsion — an interaction that is apparent in surface wetting/dewetting effects in thin films<sup>14</sup> and that was recently measured quantitatively, as described below. In the simple van der Waals picture of Fig. 1, involving two microspheres of permittivities  $\epsilon_{1,2}$  and fluctuating dipole moments  $\mathbf{p}_{1,2}$ , it is straightforward to see how the force will reverse in sign if the particles are immersed in a fluid with permittivity  $\epsilon_3$  such that  $\epsilon_1 > \epsilon_3 > \epsilon_2$ . As described previously, the electric field  $\mathbf{E}_1$  from the first particle's dipole moment  $\mathbf{p}_1$  will induce a dipole moment  $\mathbf{p}_2$  in the second particle, and for spheres in the quasi-static limit this obeys the formula  $\mathbf{p}_2 \sim (\epsilon_2 - \epsilon_3)/(\epsilon_2 + 2\epsilon_3)\mathbf{E}_1$ , which reverses sign if  $\epsilon_2 < \epsilon_3$  (ref. 10). That

is, when particle 2 is less polarizable (smaller  $\epsilon$ ) than the surrounding medium, its effective negative polarizability reverses the sign of the induced dipole moment  $\mathbf{p}_2$ , which in turn changes the sign of the force. Repulsion also requires  $\epsilon_1 > \epsilon_3$ , as otherwise both particles will have reversed dipole moments and the force will remain attractive, because the force is proportional to the product of the two polarizabilities<sup>10</sup>. Repulsion under these  $\epsilon$  conditions turns out to hold more generally in the Casimir regime, where retardation and non-additivity are present<sup>10</sup>.

As demonstrated by Dzyaloshinskiĭ, Lifshitz and Pitaevskiĭ, the sign of the Casimir force between two plates immersed in a fluid depends on the dielectric properties of the materials involved<sup>10</sup>. Two plates made from the same material will always attract, regardless of the choice of intermediate material (typically a fluid or vacuum). However, the force between slabs of different materials (here labelled '1' and '2') can become repulsive by suitable choice of the intermediate liquid (labelled '3'). Specifically, as in the van der Waals case, the condition for repulsion is

$$\epsilon_1(i\kappa) > \epsilon_3(i\kappa) > \epsilon_2(i\kappa) \quad (3)$$

where the dielectric functions  $\epsilon_i$  of the materials are evaluated at imaginary frequencies  $\omega = i\kappa$  (ref. 10), as explained above.

An easy-to-see limit for the above repulsion is the case in which region 2 is air or vacuum and region 1 is a solid substrate. In this limit, substance 3, rather than forming a droplet, spreads out to achieve maximum proximity with the substrate — a wetting effect<sup>14</sup>. Because  $\epsilon$  generally varies with frequency, it is conceivable that the above inequality may be satisfied for some frequencies and not for others. In fact, only a few material systems, mostly those consisting of two solids separated by a liquid, obey the above inequality over a large frequency range. One such solid-liquid-solid material combination comprises gold, bromobenzene and silica ( $\text{SiO}_2$ ).

In a recent experiment, the long-range repulsive Casimir force between a gold-coated sphere and a silica plate immersed in bromobenzene was measured. The silica plate was then replaced by a thick gold film, and the measurements were repeated<sup>35</sup>. The results show (Fig. 5a) that the force is attractive for a gold film but repulsive for a silica plate, which is in agreement with theoretical predictions<sup>10</sup>. A known force between the sphere and plate — the hydrodynamic force — was used to calibrate the cantilever force constant and the surface separation at contact<sup>112</sup>. Repulsive forces in systems satisfying equation (3) were previously reported in the van der Waals (quasi-static) regime, although with much larger uncertainties (see ref. 113 and references therein).

Material dispersion and geometry can conspire to induce a variety of additional effects in fluids. For example, the force can switch sign with separation because fluctuations at different wavelengths become important at different separations and  $\epsilon$  changes with wavelength, leading to unstable or stable equilibria<sup>4,95</sup>. If equation (3) is only satisfied for large  $\kappa$ , which becomes increasingly important at small separations, it is possible for the force to be repulsive at small separations and attractive at large separations<sup>95</sup>, leading to a stable point of zero force at some intermediate separation. Such stable non-touching suspensions are particularly interesting for microfluidic colloid applications or for frictionless static bearings. As shown in Fig. 5b, the equilibrium separations between objects can be tuned for a given material pair by changing the geometry, such as the sphere radii, which introduces additional wavelength dependence to the polarizability<sup>95</sup>. There has also been considerable interest in observing the temperature dependence of the Casimir force, in which changing the temperature changes the photon-fluctuation distribution and hence the force. In traditional parallel-plate geometries the temperature dependence turns out to be very small in practice<sup>59</sup> and has only recently been clearly observed<sup>33</sup>, but a

much larger temperature dependence can be designed in microfluidic suspensions<sup>114</sup>. As shown in Fig. 5c, the equilibrium separation of two suspended plates can vary rapidly with temperature and can even experience a temperature-induced bifurcation, in which the stable equilibrium completely disappears above a critical temperature<sup>114</sup>. Other large corrections to the temperature dependence have been calculated recently in geometries consisting of vacuum-separated spheres<sup>97,98</sup> or cones<sup>94</sup> and plates, although in these systems what is computed is the change in the ratio of magnitudes between the finite force and the zero-temperature force, which tends to be small at submicrometre separations. In general, many possibilities remain to be explored for temperature-tunable long-range interactions in fluids, not only for particle suspensions but also perhaps for surface-wetting phenomena and other fluid-flow problems.

**Device applications.** The development of increasingly complex MEMS will give more attention to scaling issues as this technology evolves towards NEMS (nanoelectromechanical systems). The issue of Casimir interactions between metallic and dielectric surfaces in close proximity will inevitably need to be faced, with particular attention being given to potentially troublesome phenomena such as stiction — the irreversible adhesion of moving parts resulting from electrostatic and Casimir forces<sup>115,116</sup>. On the other hand, such phenomena might be exploited to add new functionality to the architecture of NEMS.

An instructive example of the applications of Casimir forces is to use the device of Fig. 2b as a driven electromechanical oscillator. As the distance between the plate and the sphere decreases, the Casimir interaction adds a nonlinear term to the force that leads to the characteristic bistable effect evident in the resonance peak as it transforms from case I to case IV in Fig. 6a, corresponding to a hysteresis in the distance dependence shown in Fig. 6b. This Casimir anharmonic oscillator, first studied theoretically in ref. 117, functions as a nanometric sensor for measuring the separation between two uncharged metallic surfaces.

Repulsive Casimir forces could also be of significant technological interest, such as for the development of ultrasensitive force and torque sensors that levitate objects above surfaces without disturbing electric or magnetic interactions and with virtually no static friction to rotation or translation<sup>8</sup>.

### Concluding remarks

The days of considering long-range van der Waals interactions between neutral bodies as monotonic, additive and attractive with simple power laws has come to a close. Experimental work is beginning to regularly enter submicrometre regimes with microstructured materials that cannot be characterized by simple parallel- or sphere-plate results, and a recently developed experimental technique based on a force sensor is particularly promising in this regard<sup>118</sup>. Fortunately, these developments have coincided with the emergence of new theoretical tools that are rapidly exploring the potential for new phenomena outside of the additive regime. Many interesting theoretical and experimental avenues remain to be pursued in this fascinating field. For instance, many of the recent theoretical predictions of unusual Casimir physics outlined above, including non-monotonic force dependencies, repulsive forces, large temperature effects, fluid suspensions and orientation transitions arising from fluid dispersion or geometry, have yet to be observed experimentally. There are interesting theoretical predictions concerning anisotropic crystals that are awaiting experimental verification, such as the orientation-dependent Casimir force arising from highly anisotropic crystals<sup>119</sup> and the quantum electrodynamic torque between birefringent materials<sup>8,102–104</sup>. An important question is whether the Casimir force can undergo a significant change near a suitable phase transition. Interesting candidates for

this effect are materials undergoing a metal–insulator transition, as these experience large variations in the plasma frequency.

MEMS can be used to study the interplay of Casimir forces and optical forces resulting from intensity gradients, whose interplay may result in many interesting applications. Although the impact of this progress on practical devices remains to be seen, one thing is clear: compared with the vast array of geometries, materials and phenomena that have been explored for classical photonics, work on Casimir phenomena is only now beginning to scratch the surface of what may be possible.

### References

1. Israelachvili, J. N. *Intermolecular and Surface Forces* (Academic, 1991).
2. London, F. The general theory of molecular forces. *Trans. Faraday Soc.* **33**, 8–26 (1937).
3. Mahanty, J. & Ninham, B. W. *Dispersion Forces* (Academic, 1976).
4. Parsegian, V. A. *Van der Waals Forces: A Handbook for Biologists, Chemists, Engineers, and Physicists* (Cambridge Univ., 2006).
5. Ball, P. Fundamental physics: Feel the force. *Nature* **447**, 772–774 (2007).
6. Bordag, M., Mohideen, U. & Mostepanenko, V. M. New developments in the Casimir effect. *Phys. Rep.* **353**, 1–205 (2001).
7. Buhmann, S. Y. & Welsch, D.-G. Dispersion forces in macroscopic quantum electrodynamics. *Prog. Quant. Electron.* **31**, 51–130 (2007).
8. Capasso, F., Munday, J. N., Iannuzzi, D. & Chan, H. B. Casimir forces and quantum electrodynamic torques: Physics and nanomechanics. *IEEE J. Sel. Top. Quant. Electron.* **13**, 400–415 (2007).
9. Casimir, H. B. G. On the attraction between two perfectly conducting plates. *Proc. K. Ned. Akad. Wet.* **51**, 793–795 (1948).
10. Dzyaloshinskii, I. E., Lifshitz, E. M. & Pitaevskii, L. P. The general theory of van der Waals forces. *Adv. Phys.* **10**, 165–209 (1961).
11. Kardar, M. & Golestanian, R. The ‘friction’ of vacuum, and other fluctuation-induced forces. *Rev. Mod. Phys.* **71**, 1233–1245 (1999).
12. Lambrecht, A. The Casimir effect: a force from nothing. *Phys. World* **15**, 29–32 (Sept. 2002).
13. Lamoreaux, S. K. The Casimir force: background, experiments, and applications. *Rep. Prog. Phys.* **68**, 201–236 (2005).
14. Lamoreaux, S. K. Casimir forces: Still surprising after 60 years. *Phys. Today* **60**, 40–45 (2007).
15. Lifshitz, E. M. The theory of molecular attractive forces between solids. *Sov. Phys. JETP* **2**, 73–84 (1956).
16. Milonni, P. W. *The Quantum Vacuum: An Introduction to Quantum Electrodynamics* (Academic, 1993).
17. Milton, K. A. *The Casimir Effect: Physical Manifestations of Zero-Point Energy* (World Scientific, 2001).
18. Milton, K. A. The Casimir effect: Recent controversies and progress. *J. Phys. A* **37**, R209–R277 (2004).
19. Onofrio, R. Casimir forces and non-Newtonian gravitation. *New J. Phys.* **8**, 237 (2006).
20. Plunien, G., Müller, B. & Greiner, W. The Casimir effect. *Phys. Rep.* **134**, 87–193 (1986).
21. Spruch, L. Long-range Casimir interactions. *Science* **272**, 1452–1455 (1996).
22. Rodriguez, A. W., Joannopoulos, J. D. & Johnson, S. G. Repulsive and attractive Casimir forces in a glide-symmetric geometry. *Phys. Rev. A* **77**, 062107 (2008).
23. Miri, M. & Golestanian, R. A frustrated nanomechanical device powered by the lateral Casimir force. *Appl. Phys. Lett.* **92**, 113103 (2008).
24. Genet, C., Lambrecht, A. & Reynaud, S. The Casimir effect in the nanoworld. *Eur. Phys. J. Spec. Top.* **160**, 183–193 (2008).
25. Bressi, G., Carugno, G., Onofrio, R. & Ruoso, G. Measurement of the Casimir force between parallel metallic surfaces. *Phys. Rev. Lett.* **88**, 041804 (2002).
26. Chan, H. B. *et al.* Measurement of the Casimir force between a gold sphere and a silicon surface with a nanotrench array. *Phys. Rev. Lett.* **101**, 030401 (2008).
27. Decca, R. S., Lopez, D., Fischbach, E. & Krause, D. E. Measurement of the Casimir force between dissimilar metals. *Phys. Rev. Lett.* **91**, 050402 (2003).
28. Derjaguin, B. & Abrikosova, I. Direct measurements of molecular attraction of solids. *J. Phys. Chem. Solids* **5**, 1–10 (1958).
29. Ederth, T. Template-stripped gold surfaces with 0.4-nm rms roughness suitable for force measurements: Application to the Casimir force in the 20–100-nm range. *Phys. Rev. A* **62**, 062104 (2000).
30. Krause, D. E., Decca, R. S., López, D. & Fischbach, E. Experimental investigation of the Casimir force beyond the proximity-force approximation. *Phys. Rev. Lett.* **98**, 050403 (2007).

31. Lamoreaux, S. K. Demonstration of the Casimir force in the 0.6 to 6  $\mu\text{m}$  range. *Phys. Rev. Lett.* **78**, 5–8 (1997).
32. Mohideen, U. & Roy, A. Precision measurement of the Casimir force from 0.1 to 0.9  $\mu\text{m}$ . *Phys. Rev. Lett.* **81**, 4549–4552 (1998).
33. Sushkov, A. O., Kim, W. J., Dalvit, D. A. R. & Lamoreaux, S. K. Observation of the thermal Casimir force. *Nature Phys.* **7**, 230–233 (2011).
34. van Blokland, P. H. G. M. & Overbeek, J. T. G. Van der Waals forces between objects covered with a chromium layer. *J. Chem. Soc. Faraday Trans.* **174**, 2637–2651 (1978).
35. Munday, J., Capasso, F. & Parsegian, V. A. Measured long-range repulsive Casimir–Lifshitz forces. *Nature* **457**, 170–173 (2009).
36. Emig, T., Graham, N., Jaffe, R. L. & Kardar, M. Casimir forces between arbitrary compact objects. *Phys. Rev. Lett.* **99**, 170403 (2007).
37. Gies, H. & Klingmüller, K. Worldline algorithms for Casimir configurations. *Phys. Rev. D* **74**, 045002 (2006).
38. Johnson, S. G. Numerical methods for computing Casimir interactions. Preprint at <http://arxiv.org/abs/1007.0966> (2010).
39. Lambrecht, A., Maia Neto, P. A. & Reynaud, S. The Casimir effect within scattering theory. *New J. Phys.* **8**, 243 (2006).
40. McCauley, A. P., Rodriguez, A. W., Joannopoulos, J. D. & Johnson, S. G. Casimir forces in the time domain: Applications. *Phys. Rev. A* **81**, 012119 (2010).
41. Pasquali, S. & Maggs, A. C. Fluctuation-induced interactions between dielectrics in general geometries. *J. Chem. Phys.* **129**, 014703 (2008).
42. Rahi, S. J., Emig, T., Graham, N., Jaffe, R. L. & Kardar, M. Scattering theory approach to electrodynamic Casimir forces. *Phys. Rev. D* **80**, 085021 (2009).
43. Reid, M. T. H., Rodriguez, A. W., White, J. & Johnson, S. G. Efficient computation of three-dimensional Casimir forces. *Phys. Rev. Lett.* **103**, 040401 (2009).
44. Rodriguez, A., Ibanescu, M., Iannuzzi, D., Joannopoulos, J. D. & Johnson, S. G. Virtual photons in imaginary time: Computing Casimir forces in arbitrary geometries via standard numerical electromagnetism. *Phys. Rev. A* **76**, 032106 (2007).
45. Rodriguez, A. W., McCauley, A. P., Joannopoulos, J. D. & Johnson, S. G. Casimir forces in the time domain: Theory. *Phys. Rev. A* **80**, 012115 (2009).
46. Chan, H. B., Aksyuk, V. A., Kleinman, R. N., Bishop, D. J. & Capasso, F. Nonlinear micromechanical Casimir oscillator. *Phys. Rev. Lett.* **87**, 211801 (2001).
47. Casimir, H. B. G. & Polder, D. The influence of retardation on the London–van der Waals forces. *Phys. Rev.* **13**, 360–372 (1948).
48. Milton, K. A., Parashar, P. & Wagner, J. Exact results for Casimir interactions between dielectric bodies: the weak-coupling or van der Waals limit. *Phys. Rev. Lett.* **101**, 160402 (2008).
49. Sparnaay, M. Measurements of attractive forces between flat plates. *Physica* **24**, 751–764 (1958).
50. de Man, S., Heeck, K., Wijngaarden, R. J. & Iannuzzi, D. Halving the Casimir force with conductive oxides. *Phys. Rev. Lett.* **103**, 040402 (2009).
51. Kim, W. J., Sushkov, A. O., Dalvit, D. A. R. & Lamoreaux, S. K. Surface contact potential patches and Casimir force measurements. *Phys. Rev. A* **81**, 022505 (2010).
52. Munday, J. N. & Capasso, F. Reply to “Comment on ‘Precision measurement of the Casimir–Lifshitz force in a fluid’”. *Phys. Rev. A* **77**, 036103 (2008).
53. Pirozhenko, I., Lambrecht, A. & Svetovoy, V. B. Sample dependence of the Casimir force. *New J. Phys.* **8**, 238 (2006).
54. van Zwol, P. J., Palasantzas, G. & De Hosson, J. T. M. Influence of dielectric properties on van der Waals/Casimir forces in solid–liquid systems. *Phys. Rev. B* **79**, 195428 (2009).
55. Genet, C., Lambrecht, A., Maia Neto, P. & Reynaud, S. The Casimir force between rough metallic plates. *Europhys. Lett.* **62**, 484–490 (2003).
56. Maia Neto, P. A., Lambrecht, A. & Reynaud, S. Roughness correction to the Casimir force: Beyond the proximity force approximation. *Europhys. Lett.* **69**, 924–930 (2005).
57. Klimchitskaya, G. L., Mohideen, U. & Mostepanenko, V. M. The Casimir force between real materials: Experiment and theory. *Rev. Mod. Phys.* **81**, 1827–1885 (2009).
58. Decca, R. S. *et al.* Tests of new physics from precise measurements of the Casimir pressure between two gold-coated spheres. *Phys. Rev. D* **75**, 077101 (2007).
59. Brevik, I., Aarseth, J. B., Høye, J. S. & Milton, K. A. Temperature dependence of the Casimir effect. *Phys. Rev. E* **71**, 056101 (2005).
60. Derjaguin, B. V. Untersuchungen über die reibung und adhesion. *Kolloid Z.* **69**, 155–164 (1934).
61. Roy, A., Lin, C. Y. & Mohideen, U. Improved precision measurement of the Casimir force. *Phys. Rev. D* **60**, 111101(R) (1999).
62. Palasantzas, G., van Zwol, P. J. & De Hosson, J. Th. M. Transition from Casimir to van der Waals force between macroscopic bodies. *Appl. Phys. Lett.* **93**, 121912 (2008).
63. Decca, R. *et al.* Precise comparison of theory and new experiment for the Casimir force leads to stronger constraints on thermal quantum effects and long-range interactions. *Ann. Phys.* **318**, 37–80 (2005).
64. Jourdan, G., Lambrecht, A., Comin, F. & Chevrier, J. Quantitative non-contact dynamic Casimir force measurements. *Europhys. Lett.* **85**, 31001 (2009).
65. Chan, H. B., Aksyuk, V. A., Kleinman, R. N., Bishop, D. J. & Capasso, F. Quantum mechanical actuation of microelectromechanical systems by the Casimir force. *Science* **291**, 1941–1944 (2001).
66. Bostrom, M. & Sernelius, B. E. Thermal effects on the Casimir force in the 0.1–0.5  $\mu\text{m}$  range. *Phys. Rev. Lett.* **84**, 4757–4760 (2000).
67. Masuda, M. & Sasaki, M. Limits on nonstandard forces in the submicrometer range. *Phys. Rev. Lett.* **102**, 171101 (2009).
68. Klimchitskaya, G. L., Mohideen, U. & Mostepanenko, V. M. Casimir and van der Waals forces between two plates or a sphere (lens) above a plate made of real metals. *Phys. Rev. A* **61**, 062107 (2000).
69. Tomaš, M. S. Casimir force in absorbing multilayers. *Phys. Rev. A* **66**, 052103 (2002).
70. Zhou, F. & Spruch, L. Van der Waals and retardation (Casimir) interactions of an electron or an atom with multilayered walls. *Phys. Rev. A* **52**, 297–310 (1995).
71. Boyer, T. H. Van der Waals forces and zero-point energy for dielectric and permeable materials. *Phys. Rev. A* **9**, 2078–2084 (1974).
72. Derjaguin, B. V., Abrikosova, I. I. & Lifshitz, E. M. Direct measurement of molecular attraction between solids separated by a narrow gap. *Q. Rev. Chem. Soc.* **10**, 295–329 (1956).
73. Bordag, M. Casimir effect for a sphere and a cylinder in front of a plane and corrections to the proximity force theorem. *Phys. Rev. D* **73**, 125018 (2006).
74. Golestanian, R. Casimir–Lifshitz interaction between dielectrics of arbitrary geometry: A dielectric contrast perturbation theory. *Phys. Rev. A* **80**, 012519 (2009).
75. Milton, K. A. & Wagner, J. Multiple scattering methods in Casimir calculations. *J. Phys. A* **41**, 155402 (2008).
76. Boyer, T. H. Quantum electrodynamic zero-point energy of a conducting spherical shell and the Casimir model for a charged particle. *Phys. Rev.* **174**, 1764–1776 (1968).
77. Milton, K. A., DeRaad, L. L. Jr & Schwinger, J. Casimir self-stress on a perfectly conducting spherical shell. *Ann. Phys.* **115**, 388–403 (1978).
78. Cavalcanti, R. M. Casimir force on a piston. *Phys. Rev. D* **69**, 065015 (2004).
79. Hertzberg, M. P., Jaffe, R. L., Kardar, M. & Scardicchio, A. Casimir forces in a piston geometry at zero and finite temperatures. *Phys. Rev. D* **76**, 045016 (2007).
80. Marachevsky, V. N. Casimir interaction: Pistons and cavity. *J. Phys. A* **41**, 164007 (2008).
81. Kenneth, O., Klich, I., Mann, A. & Revzen, M. Repulsive Casimir forces. *Phys. Rev. Lett.* **89**, 033001 (2002).
82. Jaffe, R. L. Unnatural acts: Unphysical consequences of imposing boundary conditions on quantum fields. *Proc. AIP Conf.* **687**, 3–12 (2003).
83. Emig, T., Hanke, A., Golestanian, R. & Kardar, M. Probing the strong boundary shape dependence of the Casimir force. *Phys. Rev. Lett.* **87**, 260402 (2001).
84. Emig, T., Jaffe, R. L., Kardar, M. & Scardicchio, A. Casimir interaction between a plate and a cylinder. *Phys. Rev. Lett.* **96**, 080403 (2006).
85. Mazitelli, F. D., Dalvit, D. A. & Lobardo, F. C. Exact zero-point interaction energy between cylinders. *New J. Phys.* **8**, 1–21 (2006).
86. Lambrecht, A. & Marachevsky, V. N. Casimir interactions of dielectric gratings. *Phys. Rev. Lett.* **101**, 160403 (2008).
87. Balian, R. & Duplantier, B. Electromagnetic waves near perfect conductors II: Casimir effect. *Ann. Phys.* **112**, 165–208 (1978).
88. Dalvit, D. A. R., Lombardo, F. C., Mazitelli, F. D. & Onofrio, R. Exact Casimir interaction between eccentric cylinders. *Phys. Rev. A* **74**, 020101(R) (2006).
89. Kenneth, O. & Klich, I. Casimir forces in a T-operator approach. *Phys. Rev. B* **78**, 014103 (2008).
90. Reid, H., White, J. & Johnson, S. G. Efficient computation of Casimir interactions between arbitrary 3d objects with arbitrary material properties. Preprint at <http://arxiv.org/abs/1010.5539> (2010).
91. Xiong, J. L., Tong, M. S., Atkins, P. & Chew, W. C. Efficient evaluation of Casimir force in arbitrary three-dimensional geometries by integral equation methods. *Phys. Lett. A* **374**, 2517–2520 (2010).
92. Maia Neto, P. A., Lambrecht, A. & Reynaud, S. Casimir energy between a plane and a sphere in electromagnetic vacuum. *Phys. Rev. A* **78**, 012115 (2008).

93. Rodriguez, A. *et al.* Computation and visualization of Casimir forces in arbitrary geometries: Non-monotonic lateral-wall forces and failure of proximity force approximations. *Phys. Rev. Lett.* **99**, 080401 (2007).
94. Maghrebi, M. F. *et al.* Casimir force between sharp-shaped conductors. Preprint at <http://arxiv.org/abs/1010.3223> (2010).
95. Rodriguez, A. W. *et al.* Non-touching nanoparticle diclusters bound by repulsive and attractive Casimir forces. *Phys. Rev. Lett.* **104**, 160402 (2010).
96. Rahi, S. J. *et al.* Nonmonotonic effects of parallel sidewalls on Casimir forces between cylinders. *Phys. Rev. A* **77**, 030101(R) (2008).
97. Canaguier-Durand, A., Neto, P. A. M., Lambrecht, A. & Reynaud, S. Thermal Casimir effect in the plane-sphere geometry. *Phys. Rev. Lett.* **104**, 040403 (2010).
98. Weber, A. & Gies, H. Nonmonotonic thermal Casimir force from geometry-temperature interplay. *Phys. Rev. Lett.* **105**, 040403 (2010).
99. Kenneth, O. & Klich, I. Opposites attract: A theorem about the Casimir force. *Phys. Rev. Lett.* **97**, 160401 (2006).
100. Rahi, S. J., Kardar, M. & Emig, T. Constraints on stable equilibria with fluctuation-induced forces. *Phys. Rev. Lett.* **105**, 070404 (2010).
101. Levin, M., McCauley, A. P., Rodriguez, A. W., Reid, M. T. H. & Johnson, S. G. Casimir repulsion between metallic objects in vacuum. *Phys. Rev. Lett.* **105**, 090403 (2010).
102. Parsegian, V. A. & Weiss, G. H. Dielectric anisotropy and the van der Waals interaction between bulk media. *J. Adhesion* **3**, 259–267 (1972).
103. Barash, Y. Moment of van der Waals forces between anisotropic bodies. *Izv. Vuz. Radiofiz.* **21**, 1138–1143 (1978).
104. Munday, J. N., Iannuzzi, D., Barash, Y. & Capasso, F. Torque induced on birefringent plates by quantum fluctuations. *Phys. Rev. A* **71**, 042102 (2005).
105. Rodrigues, R. B., Maia Neto, P. A., Lambrecht, A. & Reynaud, S. Vacuum-induced torque between corrugated metallic plates. *Europhys. Lett.* **76**, 822–828 (2006).
106. Milton, K. A., Parashar, P., Wagner, J. & Pelaez, C. Multiple scattering Casimir force calculations: layered and corrugated materials, wedges, and Casimir-Polder forces. *J. Vac. Sci. Tech. B* **28**, C4A8–C4A16 (2010).
107. Rodriguez, A. W. *et al.* Stable suspension and dispersion-induced transition from repulsive Casimir forces between fluid-separated eccentric cylinders. *Phys. Rev. Lett.* **101**, 190404 (2008).
108. Duraffourg, L. & Andreucci, P. Casimir force between doped silicon slabs. *Phys. Lett. A* **359**, 406–411 (2006).
109. Lambrecht, A., Pirozhenko, I., Duraffourg, L. & Andreucci, P. The Casimir effect for silicon and gold slabs. *Europhys. Lett.* **77**, 44006 (2007).
110. Büscher, R. & Emig, T. Nonperturbative approach to Casimir interactions in periodic geometries. *Phys. Rev. A* **69**, 062101 (2004).
111. Chiu, H.-C., Klimchitskaya, G. L., Marachevsky, V. N., Mostepanenko, V. M. & Mohideen, U. Lateral Casimir force between sinusoidally corrugated surfaces: asymmetric profiles, deviations from the proximity force approximation, and comparison with exact theory. *Phys. Rev. B* **81**, 115417 (2010).
112. Munday, J. N. & Capasso, F. Measurement of the Casimir-Lifshitz force in fluids: the effect of electrostatic forces and Debye screening. *Phys. Rev. A* **78**, 032109 (2008).
113. Feiler, A. A., Bergstrom, L. & Rutland, M. W. Superlubricity using repulsive van der Waals forces. *Langmuir* **24**, 2274–2276 (2008).
114. Rodriguez, A. W., Woolf, D., McCauley, A. P., Capasso, F. & Johnson, S. G. Achieving a strongly temperature-dependent Casimir effect. *Phys. Rev. Lett.* **105**, 060401 (2010).
115. Buks, E. & Roukes, M. L. Metastability and the Casimir effect in micromechanical systems. *Europhys. Lett.* **54**, 220–226 (2001).
116. Serry, F. M., Walliser, D. & Jordan, M. G. The role of the Casimir effect in the static deflection of and stiction of membrane strips in microelectromechanical systems MEMS. *J. Appl. Phys.* **84**, 2501–2506 (1998).
117. Serry, F. M., Walliser, D. & Jordan, M. G. The anharmonic Casimir oscillator — the Casimir effect in a model microelectromechanical system. *J. Microelec. Sys.* **4**, 193–205 (1995).
118. Zuurbier, P., de Man, S., Gruca, G., Heeck, K. & Iannuzzi, D. Measurement of the Casimir force with a ferrule-top sensor. *New J. Phys.* **13**, 023027 (2011).
119. Romanowsky, M. B. & Capasso, F. Orientation-dependent Casimir force arising from highly anisotropic crystals: Application to Bi<sub>2</sub>Sr<sub>2</sub>CaCu<sub>2</sub>O<sub>8,6</sub>. *Phys. Rev. A* **78**, 042110 (2008).
120. Davids, P. S., Intravaia, F., Rosa, F. S. S. & Dalvit, D. A. R. Modal approach to Casimir forces in periodic structures. *Phys. Rev. A* **82**, 062111 (2010).
121. Saleh, B. E. A. & Teich, M. C. *Fundamentals of Photonics* (Wiley, 1991).
122. Leonhardt, U. & Philbin, T. G. Quantum levitation by left-handed metamaterials. *New J. Phys.* **9**, 254 (2007).
123. Rosa, F. S. S., Dalvit, D. A. R. & Milonni, P. W. Casimir-Lifshitz theory and metamaterials. *Phys. Rev. Lett.* **100**, 183602 (2008).
124. Zhao, R., Zhou, J., Koschny, T., Economou, E. N. & Soukoulis, C. M. Repulsive Casimir force in chiral metamaterials. *Phys. Rev. Lett.* **103**, 103602 (2009).
125. McCauley, A. P. *et al.* Microstructure effects for Casimir forces in chiral metamaterials. *Phys. Rev. B* **82**, 165108 (2010).
126. Rosa, F. S. S. On the possibility of Casimir repulsion using metamaterials. *J. Phys. Conf. Ser.* **161**, 012039 (2009).

### Acknowledgements

The authors thank D. Iannuzzi, D. Woolf, M. Ibanescu, A. P. McCauley, H. Chan, J. N. Munday, V. A. Parsegian, S. Lamoreaux, J. D. Joannopoulos, M. Kardar, R. L. Jaffe, T. Emig, D. A. R. Dalvit and M. Lissanti for collaborations and discussions.